Journal of Materials Chemistry A

Designing π-Conjugated Polymer Blends with Improved Thermoelectric Power Factors

Journal:	*Journal of Materials Chemistry A*
Manuscript ID	TA-ART-07-2019-007464.R1
Article Type:	Paper
Date Submitted by the Author:	02-Aug-2019
Complete List of Authors:	Abtahi, Ashkan; University of Kentucky, Chemistry; University of Kentucky, Physics and Astronomy Johnson , Stephen ; Transylvania University, Physics Park, So Min; University of Kentucky, Department of Chemistry; University of Kentucky, Chemical and Materials Engineering luo, xuyi; Purdue University Department of Chemistry Liang, Zhiming; University of Kentucky, Department of Chemistry Mei, Jianguo; Purdue University, Department of Chemistry; Birck Nanotechnology Center, Graham, Kenneth; University of Kentucky, Department of Chemistry

SCHOLARONE™
Manuscripts

ARTICLE

Designing π-Conjugated Polymer Blends with Improved Thermoelectric Power Factors

Received 00th January 20xx,
Accepted 00th January 20xx

DOI: 10.1039/x0xx00000x

Ashkan Abtahi,[a,b] Stephen Johnson,[c] So Min Park,[a,d] Xuyi Luo,[e] Zhiming Liang,[a] Jianguo Mei,[e] and Kenneth R. Graham[a,*]

Blending two or more π-conjugated polymers together provides a means of manipulating charge transport properties and potentially improving the performance of organic thermoelectrics. Previous results have shown that π-conjugated polymer blends can display higher Seebeck coefficients than either of the individual polymers; however, increased power factors, and ultimately improved thermoelectric performance, in polymer blends as compared to the individual polymers has not yet been demonstrated. The purpose of this work is to theoretically and experimentally probe how the electronic properties of the individual polymers influence the Seebeck coefficient, electrical conductivity, and power factor in the polymer blends. Specifically, the influence of energetic disorder, energy offsets between the transport states in the two polymers, and charge-carrier localization lengths are investigated based on a theoretical model introduced by Arkhipov and Bässler. These calculations show that gains in the power factor should be attainable when the two polymers have a small (e.g., 0.1-0.2 eV) offset in their density of states (DOS) distributions and the polymer with the higher energy DOS has a wider DOS distri-bution and a larger localization length. Experimentally, power factors in an appropriate polymer blend are demonstrated to exceed the power factors of the individual polymers by nearly two-fold. Through the applied theoretical and experimental approach, this work provides guidance in regards to the energetics, density of states, and charge-carrier mobilities for designing higher performing organic thermoelectrics with π-conjugated polymer blends.

[a] *Department of Chemistry, University of Kentucky, Lexington, Kentucky 40506, United States.*
[b] *Department of Physics, University of Kentucky, Lexington, Kentucky 40506, United States.*
[c] *Department of Physics, Transylvania University, Lexington, Kentucky 40508, United States*
[d] *Department of Chemical and Materials Engineering, University of Kentucky, Lexington, Kentucky 40506, United States*
[e] *Department of Chemistry, Purdue University, West Lafayette, Indiana 47907, United States*

† Footnotes relating to the title and/or authors should appear here.
Electronic Supplementary Information (ESI) available: [details of any supplementary information available should be included here]. See DOI: 10.1039/x0xx00000x

Introduction

Increasing energy efficiency and providing continuous power for remote sensors or wearable electronic devices is a continuously growing challenge. Thermoelectric (TE) devices are an appealing technology to address this challenge, as these devices can convert waste heat produced by various mechanical, chemical, biological and other processes into electricity.[1–3] Inorganic TE materials such as bismuth chalcogenides and lead telluride have been studied for half a century and show relatively high performance over a wide temperature range, but the high cost of materials and device fabrication, as well as their rigid form factors, have limited their practical use.[4,5] Organic semiconductors, and particularly π-conjugated polymers, are emerging as promising alternative TE materials for low grade waste heat recovery owing to the use of potentially low-cost materials and fabrication methods, mechanical flexibility, and low weight.[6–12]

The maximum energy conversion efficiency achievable by a TE device is proportional to the thermoelectric figure of merit ZT, $ZT = T\frac{S^2\sigma}{\kappa}$, where S is the Seebeck coefficient, σ the electrical conductivity, κ the thermal conductivity and T the temperature.[13] The Seebeck effect refers to the electromotive force created by a temperature difference across a material, with S defined as the electrical potential difference induced by a $1\ K$ temperature differential (with units of volt per Kelvin). The Seebeck coefficient is determined by the average energy of charge carriers (with respect to the Fermi energy) contributing to the electrical conductivity at a certain temperature. Since polymers are generally poor thermal conductors, and have similar thermal conductivity (0.1-0.3 $Wm^{-1}K^{-1}$),[11,14–18] the power factor ($P=S^2\sigma$) is the primary metric that must be improved to increase the efficiency of organic TE devices.

Most intrinsic π-conjugated polymers have low electrical conductivities, which limits their TE performance. By introducing additional charge carriers in π-conjugated polymers, typically through molecular doping, σ increases significantly and they can reach reasonably high TE performance, with record ZT values in the range of 0.1-0.42 at room temperature, with some uncertainty due to potential artifacts arising from the Seebeck coefficient measurement geometry.[11,19,20] Increasing the charge carrier concentration, as is typically accomplished through increasing the dopant concentration, can lead to higher σ, but the increase in σ typically comes at the expense of S. This trade-off between σ and S limits the power factor.[12,17,21,22] Commonly, σ in π-conjugated polymers varies much more drastically than S, which has driven extensive efforts to increase σ by choosing different dopants,[6,11,17,19,21,23–26] manipulating the doping method,[12,27,28] designing new polymer structures,[6,29,30] or varying the material processing conditions.[8,9,17,21,22]

Another method to improve the power factor of both organic and inorganic TE materials is through manipulating the density of states (DOS),[31–33] such as may be accomplished by blending two different polymers or a polymer with carbon nanotubes or graphene.[34,35] These blend systems provide a potential means to surpass the power factors of the individual materials imposed by the trade-off between σ and S. The idea with polymer blends is that by adding a polymer with a different energetic distribution of states to the initial polymer, the energy difference between the Fermi energy and the transport states can be more controllably adjusted and even increased. To date, this approach has primarily led to higher Seebeck coefficients in blends of π-conjugated polymers, but not significantly higher power factors. Previously Zuo *et al.*[36] showed that by blending different polymers the Seebeck coefficient in the blend can surpass S of the individual polymers. In their work, blends of P3HT-$_{0.1}$:PTB7$_{0.9}$ and P3HT$_{0.05}$:TQ1$_{0.9}$ reached S of ≈1100 μVK^{-1} and ≈2000 μVK^{-1}, which surpassed S for the single polymers (S_{P3HT}=142 μVK^{-1}, S_{PTB7}=469 μVK^{-1} and S_{TQ1}=1560 μVK^{-1}). Conceptually, the polymer with the lower energy states can pin the Fermi energy, which results in the other polymers DOS lying further from the Fermi energy. When the polymer with the lower energy states is included at a low concentration, a significant amount of transport may occur through the material with states at higher energies with respect to the Fermi energy. Thus, the charge carriers contributing to σ have a higher average energy and S increases.[31,32,36]

The Seebeck coefficient is not only determined by the distribution of the mobile charge carriers relative to the Fermi energy; rather, it is determined by how the charge carriers in these different energy states contribute to the total electrical conductivity. In other words, S is determined by the energy dependence of σ. Thus, the Seebeck coefficient should increase as the mobility of higher energy charge carriers increases relative to the mobility of lower energy charge carriers. Polymer blends provide an ideal platform for systematically manipulating the energy dependence of charge transport through blending polymers with different transport energies and charge-carrier mobilities. In this work we combine theory and experiments to investigate how the mobility ratio between the polymers, combined with the energy offsets between the DOS distributions and the width of the DOS distributions, contribute to the Seebeck coefficient, electrical conductivity, and the power factor in polymer blends. Notably, processing conditions, dopant choice, polymer structures, and film morphology will also all influence the thermoelectric properties in these blends, but they are beyond the scope of this current work.

From the theoretical side, we apply a slightly modified version of the model introduced by Arkhipov and Bässler to model how transport occurs in a single polymer and in polymer blends.[37] In this model we use the Miller-Abrahams jump rate equation to account for jump distance and

This journal is © The Royal Society of Chemistry 20xx

Please do not adjust margins

energetic differences between localized states, combined with Gaussian disorder, to model charge carrier transport in organic semiconductors.[38] Using this model, we primarily focus on how the width of the DOS, the localization length, and the energy offset between the DOS of the different polymers in the blend impact *S*, *σ*, and the power factor. We find that in a single polymer a narrow DOS is the most important requirement for achieving high power factors. Calculations of polymer blends show that power factors can be improved over both individual polymers. For this improvement to be realized, the polymer with its DOS centered at a higher energy should have a higher localization length and broader DOS than the polymer with its DOS centered at a lower energy. Experimentally, we investigate 3 different polymer blend systems, where in each blend the ratio of the two polymers is varied from 1:0 to 0:1. Our experimental results are in agreement with theoretical predictions and show that power factors in polymer blends can indeed exceed those of the individual polymers at the same doping concentrations.

Theoretical Results and Discussion

I. Theoretical Model

Since the discovery of electrically conducting polymers, many groups have investigated charge transport in disordered systems using different models of transport mechanisms.[6,27,32,37,39–46,46–60] In π-conjugated polymers, charge transport occurs through jumping between localized states that are typically described as having a Gaussian distribution, especially at high charge-carrier concentrations when most of the low energy trap states are populated.[37,40,41,45,61–63] The jump rate between these states depends on both the spatial distance, localization length, and energy difference between an occupied starting state and the nearby unoccupied target states.[37,40,41,46,47] Using the generalized Einstein equation we can calculate the average charge-carrier mobility as a function of the energy of the charge carrier and from there we can calculate *σ* and *S*.[37,51]
The Gaussian DOS is given by Equation 1:

$$g(E) = \frac{N_t}{\sqrt{2\pi}\Delta} exp[-\frac{(E-E_0)^2}{2\Delta^2}] \quad (1)$$

Where *g(E)* is the distribution of states as a function of energy, N_t is the total number of states per unit volume, Δ is the width of the DOS, and E_0 is the mean energy of all states. N_t for most polymers is usually in the range of 10^{20}-10^{21} cm^{-3} and Δ, which is a characteristic of the energetic disorder,[64] is in the range of a few K_BT (K_B is the Boltzmann constant).[41,45,51,63,64] We use the Miller-Abrahams jump rate equations to explain the jump rate (υ) between states, as given by Equation 2:[38,41,60]

$$\upsilon(r_{ij}, E_i, E_j) = \upsilon_0 Exp[-R(r_{ij}, E_i, E_j)] = \upsilon_0 Exp\left[-2\frac{r_{ij}}{\alpha} - \frac{(E_j-E_i)+|E_j-E_i|}{2\,K_BT}\right] \quad (2)$$

Where v_0 is the attempt to jump frequency, R the hopping parameter, α the localization length, r_{ij} the jump distance, and E_i and E_j are energies for the starting and final states of a charge carrier. The localization length defines the decay length between wave functions of localized states, which for polymers are generally in the range of 1 to 5 Å. [33,41,46,58,59,65,66] To make a connection between α and the DOS, we define a parameter called the intrinsic length a ($a=N_t^{-1/3}$). The intrinsic length has the same units as α, as it is defining an average length between localized states. In a polymer, α is expected to be smaller than a.[41,45,46,51,63,65] In the model introduced by Arkhipov and Bässler, which we use in this work to calculate the energy dependent mobility of charge carriers, the average number of available hoping sites for a charge carrier starting at energy E_i whose hopping parameter is smaller than R is calculated by Equation 3.

$$n(E_i, R) = \frac{\pi}{6}\alpha^3 R^3 \left(\int_{-\infty}^{E_i} g_u(E_j, E_F) dE_j + \int_{E_i}^{E_i + K_BT\,R} g_u(E_j, E_F)\left(1 - \frac{E_j - E_i}{K_BT\,R}\right)^3 dE_j\right) \quad (3)$$

Here, $g_u(E,E_F)$ is the density of unoccupied states and E_F is the Fermi energy. The density of unoccupied states is calculated using the Fermi-Dirac distribution:

$$g_u(E, E_F) = g(E)(1 - f_{FD}(E, E_F)) \quad (4)$$

Where f_{FD} is the Fermi-Dirac distribution ($f_{FD}(E, E_F) = (1 + Exp(\frac{E-E_F}{K_BT}))^{-1}$). The Fermi energy can be determined by solving the following equation:

$$N_C = \int_{-\infty}^{\infty} g(E)\, f_{FD}(E, E_F)\, dE \quad (5)$$

Where N_C is the total number of charge carriers per unit volume. For simplicity, in this study we neglect the effect of backwards jumps.[37] By using a Poisson distribution, the average hopping parameter $\langle R \rangle$ and average squared jump distance $\langle r^2 \rangle$ can be calculated, and from there we calculate the energy dependent mobility, $\mu(E)$, using the Einstein relationship (detail of this calculation can be found in SI section II Arkhipov-Bässler model) :

$$\mu(E) = \frac{e\upsilon_0}{K_BT}\langle r^2 \rangle(E)\, Exp[-\langle R \rangle(E)]\,(1 - f_{FD}(E, E_F)) \quad (6)$$

Where e is the elementary charge. Using the energy dependent mobility, the average charge-carrier mobility and electrical conductivity can be calculated with Equations 7 and 8.

$$\bar{\mu} = \frac{1}{N_C}\int_{-\infty}^{\infty} g(E)\, f_{FD}(E, E_F)\mu(E)\, dE \quad (7)$$

$$\sigma = eN_C\bar{\mu} = \int_{-\infty}^{\infty}\sigma(E)dE = e\int_{-\infty}^{\infty} g(E)\, f_{FD}(E, E_F)\mu(E)\, dE \quad (8)$$

The Seebeck coefficient is proportional to the average energy (with respect to the Fermi energy) of conducting charge-carriers weighted by their contribution to the total electrical conductivity, as given by equation 9.

$$S = \frac{1}{Te}\int_{-\infty}^{\infty}\frac{\sigma(E)}{\sigma}(E - E_F)dE = \frac{1}{Te}(E_T - E_F) \quad (9)$$

Here, the transport energy, E_T, is the average energy of charge carriers weighted by their contribution to the total

electrical conductivity. To allow more direct comparison between π-conjugated polymers with varying charge-carrier mobility and DOS distributions, the total density of charge carriers is kept constant in further calculations. The other two remaining parameters, the localization length and DOS width, are variable. To make the calculations as comparable as possible, we keep the ratio between the average distance between states (a) and α constant in our initial calculations.

II. Single Polymer

Figure 1a and b show the results of calculations performed with equations 8 and 9 as a function of the width of the DOS and α. The intrinsic length is calculated such that the total number of states is between 1×10^{20} and 1×10^{21} cm^{-3} and $\frac{a}{\alpha}$ adjusted such that $\frac{a}{\alpha}$ equals 10. Changing the $\frac{a}{\alpha}$ ratio does affect the trends in TE properties and further discussion can be found in the SI, section III. The results presented in Figure 1a show that as the DOS narrows for a particular localization length σ increases and S decreases. Additionally, as α increases for a given DOS width, σ increases and S decreases. Figure 1b shows that the power factor increases by approximately two orders of magnitude as the DOS width of the polymer decreases from 6 to 1 K_BT, which is primarily attributed to the change in σ. A more specific discussion follows to rationalize the various trends, but in general the modeling shows that for a single polymer it is most beneficial to have a narrow DOS.[46,51,64] Although the trends are accurate, the absolute value of the electrical conductivity will depend heavily on the value of ν_0.

The increase in σ with narrowing of the DOS is rationalized by considering that on average there will be more available states nearby that are energetically accessible for a charge carrier to jump to. To put it more quantitatively, according to Eq. 2 a smaller energetic offset in a jump will lead to an exponential increase in the jump rate. The decrease in S with decreasing width of the DOS can be explained by considering that charge carriers at lower energies will contribute more to the electrical conductivity in a narrow DOS. As illustrated in Figure 1c, when the DOS is narrow the average transport energy is lower since there are more lower energy states available for the carriers to move through. By contrast, when the DOS is wide charge carriers are forced to move through higher energy states more often due to a lack of nearby lower energy states.

Figure 1a also shows that as the localization length increases for a particular DOS width, σ increases and S decreases. The increase in σ is rationalized by the increased available sites to hop to (i.e., the charge carrier can access more states due to the larger localization length), while the decrease in S arises from a lowering of the average transport energy due to the ability to access more lower energy states from a given site. Figure 1d illustrates two cases, one with a larger localization length (blue arrows) and one with a smaller localization length (red arrows). If these two polymers have the same DOS width, the one with the larger localization length will allow a charge carrier to access more states around it. As a result, in the polymer with the larger localization length transport will occur on average through lower energy states and S will be smaller. Regardless of the DOS width, going from a localization length of 1 Å to 1.7 Å results in a similar S change of *ca.* 150 μVK^{-1}. By contrast, the changes in electrical conductivity resulting from the increased localization length are much more pronounced when the DOS is broader.

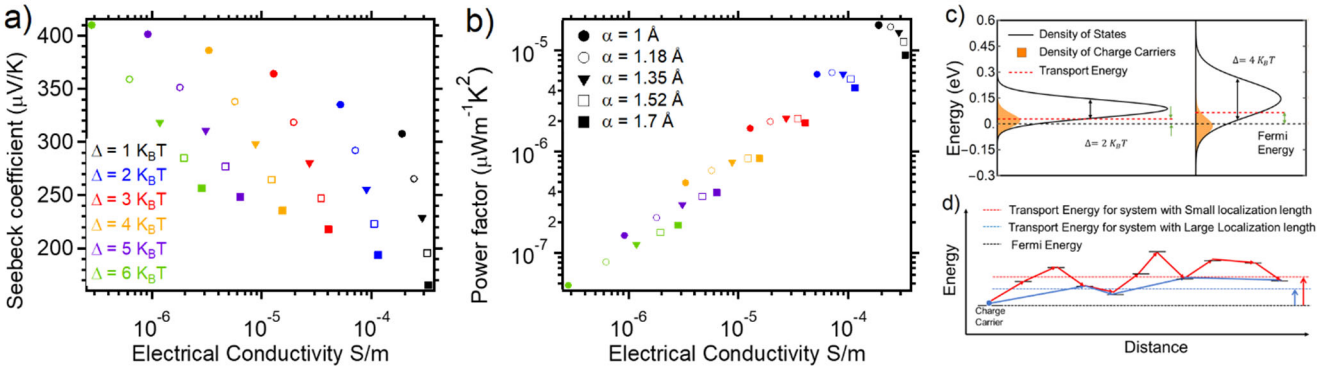

Figure 1. (a) Seebeck coefficient and (b) power factor as a function of electrical conductivity for varying DOS widths (indicated by color) and localization lengths (indicated by symbol). Here $N_C=3\times10^{19}$ cm^{-3}, $\nu_0=10^{12}$ s^{-1}, a has values of 1, 1.18,1.35, 1.52 and 1.7nm (correspondent to N_t=10, 6.09, 4.06, 2.85 and 2.06 $\times10^{20}$ cm^{-3}), Δ has values of 1-6K_BT and α values of 1,1.18, 1.35, 1.52, and 1.7 Å. For each point, the intrinsic length is chosen so $\frac{a}{\alpha}=10$. (c) Schematic illustration comparing average transport energy of two DOS distributions with the same α but different DOS widths. (d) Schematic illustrating how α affects the average transport energy.

The primary variable influencing the power factor is the DOS width, which is consistent with previous findings.[51,52] As the DOS width decreases from 6 to 1 K_BT, the power factor increases by a factor of 100. Interestingly, the trend in power factor with localization length variations is not consistent across the varying DOS widths. For a broad DOS the greatest localization length leads to the highest power factor, whereas for a narrow DOS the smallest localization length gives rise to the highest power factor. This trend arises due to the larger influence of the localization length on σ for the broad DOS relative to the narrow DOS. For a broad DOS (6 K_BT), as the localization length increases from 1 to 1.7 Å, σ increases by a

This journal is © The Royal Society of Chemistry 20xx

Please do not adjust margins

factor of 10 and *S* decreases by a factor of 1.6. As a result of the large changes in σ, the power factor increases with localization length when the DOS is broad. On the other hand, for the narrow DOS (1 K_BT) as the localization length increases from 1 to 1.7 Å, σ increases by a factor of 1.7 and *S* decreases by a factor of 1.9. Owing to the dependence of the power factor on S^2, the increase in electrical conductivity with increasing localization length is outweighed by the decrease in the Seebeck coefficient and the power factor reaches a maximum at lower localization lengths when the DOS is narrow.

III. Polymer Blends

Our model of polymer blends expands upon the single polymer model described in Section II. The two polymers are treated as a homogenous blend and the total density of states is described by Equation 10.

$$g_{blend}(E) = C_A g_A(E) + C_B g_B(E) = C_A \frac{N_{t,A}}{\sqrt{2\pi}\Delta_A} Exp\left[-\frac{(E-E_{0,A})^2}{2{\Delta_A}^2}\right] + C_B \frac{N_{t,B}}{\sqrt{2\pi}\Delta_B} Exp[-\frac{(E-E_{0,B})^2}{2{\Delta_B}^2}] \quad (10)$$

Where *C* is the concentration of polymer and the indices A and B refer to the different polymers in the blend ($C_A+C_B=1$). The average number of available hoping sites is described with Equation 11.

$$n(E_i,R) = \frac{\pi}{6}R^3\left(C_A{\alpha_A}^3\int_{-\infty}^{E_i} g_{u,A}(E_j,E_F)dE_j + \int_{E_i}^{E_i+K_BTR} g_{u,A}(E_j,E_F)\left(1-\frac{E_j-E_i}{K_BTR}\right)^3 dE_j\right) + \frac{\pi}{6}R^3\left(C_B{\alpha_B}^3\int_{-\infty}^{E_i} g_{u,B}(E_j,E_F)dE_j + \int_{E_i}^{E_i+K_BTR} g_{u,B}(E_j,E_F)\left(1-\frac{E_j-E_i}{K_BTR}\right)^3 dE_j\right) \quad (11)$$

The first term correlates with polymer A and second term is for polymer B. Unoccupied states are denoted as $g_{u,A}$ or $g_{u,B}$, ($g_{u,i}(E,E_F) = g_i(E)(1-f_{FD}(E,E_F))$). The Fermi energy is derived from equation 5, but instead of equation 1, equation 10 is used. For simplicity, the DOS in the blends is treated as a linear combination of the individual polymer DOS, which neglects any broadening or energetic shifts that may occur as a result of interactions between the different polymers. Experimentally, ultraviolet and inverse photoelectron spectra of organic semiconductor blends have been fit well with a linear combination of the two individual pure materials, albeit the energies of the individual components can shift in the blends.[67,68] Equations S6 and S8 are used to find the average jump parameter and the average squared jump distance. These parameters are then used to calculate the energy dependent mobility using equation 6, followed by the charge carrier mobility, σ, and *S* using equations 7, 8 and 9.

According to equation 11, the localization length of initial states is neglected, i.e., the available hopping sites are determined based on the energy distribution and localization length of the final states. Since we have two different polymers, the hopping parameter for a jump from polymer A to B should be different from a jump from polymer A to A. To more appropriately account for jumps between polymer A and polymer B, we have extended equation 11 to include the probability of the charge carrier starting from polymer A or polymer B and an effective localization length that accounts for jumps between polymer A and polymer B, as discussed in detail in SI section V. Based on SI Figure S6 and S7 and the discussion in SI section V, we conclude that including these additional parameters to account for jumps between polymers A and B changes the absolute values of the TE properties and results in maximum TE power factors in the blends occurring with slightly different parameters, but they do not change the general trends or resulting conclusions. For simplicity, we use equation 11, for the bulk of the discussion herein.

The equations for modeling the polymer blends include 10 independent variables at a constant temperature: C_B, $N_{t,A}$, $N_{t,B}$, Δ_A, Δ_B, $E_{0,B}$ - $E_{0,A}$ (ΔE_0), α_A, α_B, N_C and v_0. To make the results as directly comparable as possible, we keep the concentration of charge carriers constant at 3×10^{19} cm^{-3} and $v_0=10^{12}$ s^{-1}, as we did for a single polymer. The concentration of polymer B is varied from 0 to 100% in increments of 2.5%, which provides sufficient resolution to display general trends. The total number of states in the polymer blends is kept constant, which leaves 5 independent variables, Δ_A, Δ_B, α_A, α_B and ΔE_0. The DOS width is varied between 1.5 and 6 K_BT and α between 1 and 5 Å. The DOS width and α of polymer A are kept constant near the middle of the range, Δ_A=2.5 K_BT and α=2.5 Å. The DOS width and α of polymer B are varied through the specified ranges and ΔE_0 is set to 0.15eV. These parameters allow analysis of a wide range of scenarios with varying DOS widths and charge-carrier mobility ratios.

When two polymers are blended together the Fermi energy relative to the individual polymers DOS distributions will vary, and thereby the average transport energy of the charge carriers will change. This variation in the Fermi energy obtained through blending two polymers together was the motivation for the Katz group's initial work on polymer blend thermoelectrics.[31] Figure 2a and b, as well as SI Figure S3 depict how the Fermi energy changes as the polymer blend composition changes when ΔB is broad (6 KBT) and narrow (1.5 KBT), respectively, with a constant ΔE0 of 0.15 eV. As is evident, when the DOS of polymer B is broad, there is minimal change in the Fermi energy as the concentration of polymer B increases. Alternatively, when the DOS of polymer B is narrow there is a relatively large change (0.18 eV) in the position of the Fermi energy as the blend composition is varied. Accounting for the Fermi energy relative to the DOS in these two situations, when ΔB is broad the charge carriers will be relatively distributed between the two polymers; however, when ΔB is narrow most charge carriers will remain on polymer A. Thus, polymer A will dominate charge transport until polymer B reaches high concentrations. Intuitively, it can be expected that when one polymer dominates charge transport it is unlikely that the power

factor in the blends will improve over the single polymers. Thereby, we expect that the most likely scenario to show an improved power factor for the blends is one where the Fermi energy changes gradually and charge carriers are distributed over both polymers.

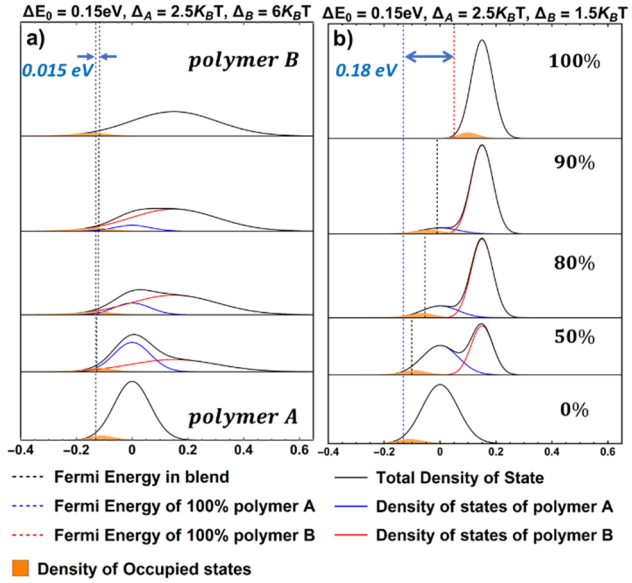

Figure 2. DOS of two polymer blends with varying compositions. In (a) the polymer with its DOS centered at higher energies has a broader DOS than the polymer with its DOS centered at lower energies and in (b) the polymer with the higher energy DOS has a narrower DOS. In both cases the DOS distributions of the polymers display a 0.15 eV energy offset.

Figure 3 shows how the calculated *S*, *σ*, and power factor vary as a function of the DOS width and *α* of polymer B. Here, the DOS width and *α* of polymer A are kept constant at 2.5 K_BT and 2 Å, respectively. In pure polymer A *S* is 190 μVK^{-1} and *σ* is 0.005 Sm^{-1}, while in pure polymer B *S* is 377, 240, and 217 μV/K and *σ* is 6.2×10^{-8} Sm^{-1}, 0.035 Sm^{-1} and 0.12 Sm^{-1} for localization lengths of 1, 4, and 5 Å, respectively. The primary findings from these calculated parameters are 1) when the DOS of polymer B is narrow, the Seebeck coefficient in the blend can exceed that of either polymer by *ca*. 60%; 2) the Seebeck coefficient improvements in the blend are higher when polymer B has a larger delocalization length; 3) electrical conductivity improvements are only seen when polymer B has a broad DOS ($6K_BT$) and a large localization length; and 4) power factors in the blend can surpass the power factors of the pure polymers when polymer B has a broad DOS and larger localization length.

When polymer B has a narrower DOS and higher localization length, an improvement in *S* appears in the blends. This observation is similar to results presented by Zuo et al.[36] and J. Sun et al.[69] The improvements are more pronounced when the DOS of polymer B is narrower and the localization length of polymer B is greater. These trends can be rationalized by considering the energy separation between the Fermi energy and the available states in polymer B combined with the charge transport properties of polymer B. As highlighted in Figure 2, the energetic separation between the DOS of polymer B and the Fermi energy increases as Δ_B becomes narrower. When the electronic states in polymer B are further separated from the Fermi energy and have higher localization lengths than states in polymer A, the average energy (transport energy) of charge carriers that contribute to conduction increases. In other words, when states at higher energies with higher charge-carrier mobilities are introduced *S* increases. The transport and Fermi energies for the blends with varying DOS width and α, as shown in SI Figure S4, highlight how both DOS width and α impact the transport energy relative to the Fermi energy and thereby the Seebeck coefficient.

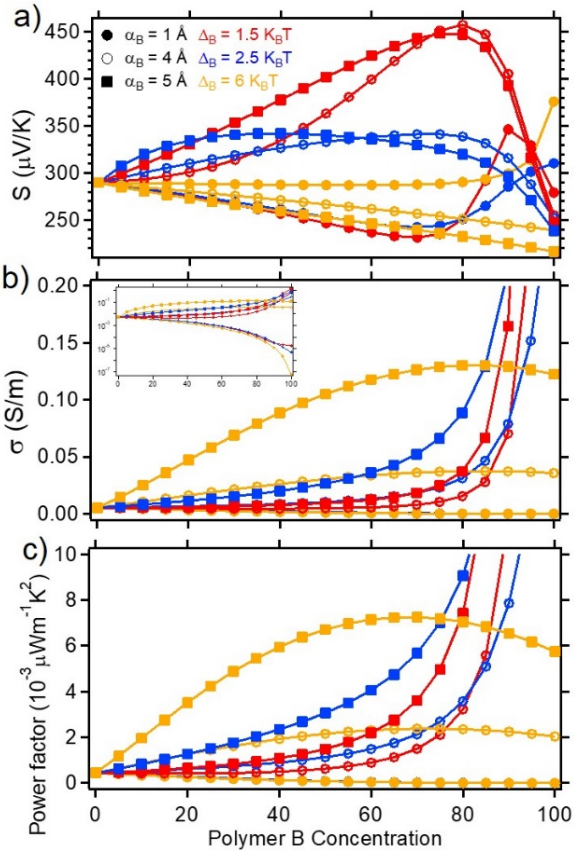

Figure 3. (a) Seebeck coefficient, (b) electrical conductivity and (c) power factor of polymer blend systems. Polymer A has fitting parameters of αA=2 Å, Nt,A= 6.1×1020 cm-3, ΔA=2.5 KBT and E0,A=0 eV and polymer B has fit parameters of αA=1,4 and 5 Å, Nt,B= 6.1×1020 cm-3, ΔA=1, 2.5 and 6 KBT and E0,B=0.15 eV (ΔE0=0.15 eV). Other fit parameters are ν0=1012s-1, T=300 K and NC=3×1019 cm-3.

Although the Seebeck coefficient in the blends increases as Δ_B decreases, the opposite is true for *σ*. As highlighted in Figure 2, the separation between the DOS of polymer B and the Fermi energy increases with decreasing DOS width, and thus there are less charge carriers populating the states on polymer B. On the other hand, Figure 3b shows that when Δ_B is broad ($6K_BT$) the electrical conductivity of the blend can slightly exceed the electrical conductivity of either of the two pure polymers. As a result of the increased electrical conductivity and Seebeck coefficient trend, the power factor

This journal is © The Royal Society of Chemistry 20xx

Please do not adjust margins

for blends with a Δ_B of 6K_BT and α_B of 4-5 Å exceed those of either of the individual polymers. For the parameters examined in Figure 3, the highest power factor gains in the blend relative to the two polymers independently is *ca.* 20% and occurs for Δ_B=6K_BT and α_B=5 Å.

A more complete analysis of how the TE properties of polymer blends vary as a function of polymer concentration (x-axis) and mobility ratio of added polymer (y-axis) to the host polymer ($\frac{\bar{\mu}_B}{\bar{\mu}_A}$) is displayed in Figure 4. Here, we compare TE properties based on the mobility ratio since it is an experimentally measurable parameter and therefore provides a more concrete guide for selecting polymers. As displayed in equations 3 and 6, the charge-carrier mobility in a single polymer increases as α increases or the DOS narrows. In these calculations, polymer A has a localization length of 2 Å and DOS width of 2.5 K_BT with $N_{t,A}$= 6.1×10^{20} cm^{-3} (a_A=1.18 nm) which gives a ratio of $\frac{a}{\alpha} = 5.9$. The maximum of the DOS for polymer B is located at 0.15 eV above the maximum of the DOS of polymer A. To study the effects of energetics and localization length on the TE properties, the total number of states and charge carrier density are kept constant in all calculations. A wide range of localization lengths (from 0.9 to 5 Å) for polymer B are used so the ratio of $\frac{a}{\alpha}$ will range from 3.5 to 18. As discussed in SI section 1b, $\frac{a}{\alpha}$ ratios above 3 lead to reasonable results. Each column in Figure 4 represents a constant DOS width for polymer B and varying localization lengths. For a constant Δ_B, the localization length is the parameter that affects the mobility. Thus, higher localization lengths correspond to higher mobility and higher mobility ratios between polymers B and A.

Focusing on the Seebeck coefficient, Figure 4a shows that blending a polymer with a narrower DOS width at higher energies will lead to up to a 58% improvement in *S* in the blends compared to the pure polymers. The gain in *S* in the blends relative to the pure polymers increases as the charge-carrier mobility of polymer B increases. This result is in line with expectations, as the relative contribution of the higher energy charge carriers to σ increases as the mobility of those higher energy charge carriers increases. As Δ_B increases to 2.5 K_BT (SI Figure S5), the increase in *S* in the blends becomes smaller, and at 6K_BT *S* no longer increases for the blends. For this wide DOS, the Seebeck coefficient changes gradually to lower values as the concentration of polymer B is increased with mobility ratios above 1. However, when the mobility ratio decreases below 1 the Seebeck gradually increases to higher values as the concentration of polymer B is increased. These trends arise due to the influence of localization length on transport and the Seebeck coefficient, as discussed previously and highlighted in Figure 1d.

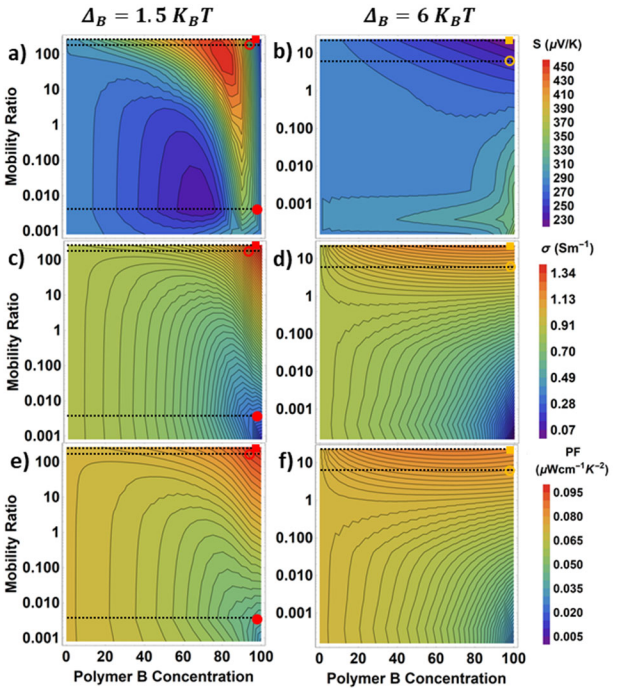

Figure 4. (a,b) Seebeck coefficient, (c,d) electrical conductivity, and (e,f) power factor calculated for polymer blends. Polymer A fitting parameters are αA=2Å, Nt,A= 6.1×1020 cm-3, ΔA=2.5 KBT and E0,A=0 eV. Each column has a different DOS width for polymer B, ΔB=1.5 KBT (a,c,e), and ΔB=6KBT (c,d,f). The other parameters for polymer B are Nt,B= 6.1×1020 cm-3 and E0,B=0.15eV (ΔE0=0.15eV) and the common parameters are ν0=1012s-1, T=300K and NC=3×1019 cm-3. The results for ΔB=2.5KBT can be found in SI figure S5. Dashed lines correspond to the data presented in Figure 3. One data line for ΔB=6KBT was less than 10-3, which is out of the range shown in the heat map.

The electrical conductivity varies more drastically across the blend composition space when Δ_B is smaller and when the mobility ratio is further from 1. Furthermore, σ varies over a much greater range than the Seebeck coefficient, as discussed previously in regards to Figure 3. Therefore, in the blends with Δ_B of 1.5 and 2.5 the electrical conductivity changes more drastically and dominates the power factor, which results in maximum power factors occurring for either pure polymer A or pure polymer B. On the other hand, when Δ_B is 6 K_BT the maximum power factors are reached with a mixture of both polymer A and polymer B. Overall, these models show that power factor enhancements over pure polymers should be attainable in polymer blends with the right combination of energy offset, DOS widths, and charge-carrier mobility differences.

Experimental Results and Discussion

We selected polymers for this study with varying charge-carrier mobilities, ionization energies (IE), and extents of disorder, as shown in Figure 5. Regioregular and regiorandom poly(3-hexylthiophene) (*RR*-P3HT and *RRa*-P3HT, respectively) are structurally similar polymers with charge-carrier mobilities that differ by several orders of magnitude and IEs that differ by *ca.* 0.2 eV.[26,70] The hole mobility of *RR*-P3HT can reach 0.1 $cm^2V^{-1}s^{-1}$ and we have measured its IE to

be 4.56±0.05 eV.[71] On the other hand, *RRa*-P3HT has a lower hole mobility of 10^{-5}-10^{-4} $cm^2V^{-1}s^{-1}$ and a higher IE of 4.73±0.05 eV.[72] The other two polymers are based on diketopyrrolopyrrole (DPP) and thiophene units and show high hole mobilities of *ca*. 1 $cm^2V^{-1}s^{-1}$,[73,74] and have similar IEs of 5.03±0.05 and 5.09±0.05 eV for PDPP-4T and PDPP-T-TT-T, respectively. With PDPP-4T and PDPP-T-TT-T both having relatively high IEs, we use the dopant molybdenum tris-[1,2-bis(trifluoromethyl) ethane-1,2-dithiolene] ($Mo(tfd)_3$),[75] which we recently measured by inverse photoemission spectroscopy to have an EA of 5.59 eV.[26] All polymer blends are doped at *ca.* 10% by volume in an attempt to maintain similar charge-carrier concentrations. In this series of blends, PDPP-4T serves as the host polymer and the polymer blended with PDPP-4T is varied. The measured *S* and *σ* values for the three different blend systems are presented in Figure 6.

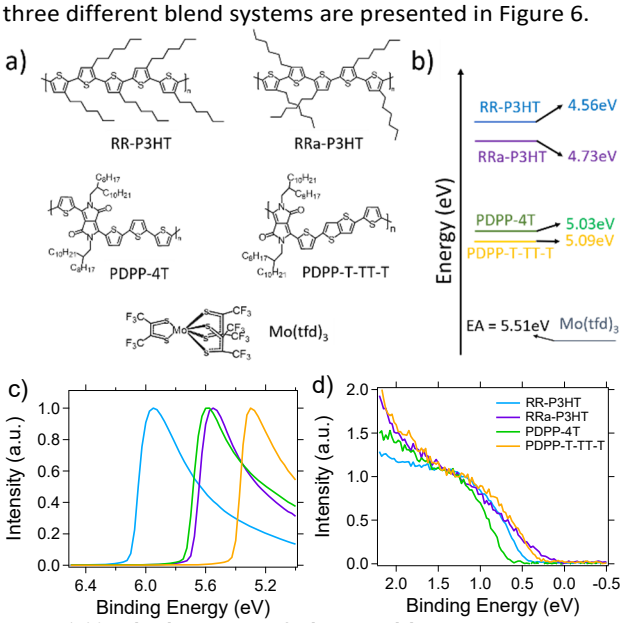

Figure 5. (a) Molecular structure of polymers and dopant, RR-P3HT, RRa-P3HT, PDPP-4T, PDPP-T-TT-T and Mo(tfd)3. (b) Ionization energy (IE) of polymers and electron affinity (EA) of dopant[26]. Normalized (c) secondary cutoff and (d) HOMO onset regions of undoped polymers measured by ultraviolet photoemission spectroscopy (UPS).

In the first case, PDPP-4T is blended with *RR*-P3HT. Here, there is a large offset between the IEs of the two polymers and the higher IE polymer, PDPP-4T, has a hole mobility that is approximately an order of magnitude greater than that of *RR*-P3HT. In the second case, PDPP-4T is blended with *RRa*-P3HT. In this case there is a large energy offset between the two polymer IEs and the lower IE polymer, *RRa*-P3HT, has a hole mobility that is three to four orders of magnitude lower than that of PDPP-4T. In the final case PDPP-4T is blended with PDPP-T-TT-T. In this blend the IE difference between the polymers is small and both polymers display similar charge-carrier mobilities. PDPP-4T:*RR*-P3HT follows one of the theoretically predicted guidelines for observing enhanced PFs in the blends, i.e., the polymer with the higher IE has a charge-carrier mobility that is an order of magnitude higher than that of the mobility in the lower IE polymer. According to the theoretical modeling, the other two blends do not have electronic properties that would lead to enhanced power factors.

The PDPP-4T:*RR*-P3HT blend indeed shows an improvement in power factor, as the blend with 85% PDPP-4T displays a power factor that is nearly double that of the pure polymers. At 10% doping by volume, pure PDPP-4T displays an electrical conductivity (52 Sm^{-1}) that is four times lower than pure *RR*-P3HT (223 Sm^{-1}) at the same doping ratio. In this blend the increase in *S* and decrease in σ are more comparable, which means that neither parameter will overwhelm the power factor. These more gradual changes lead to a higher power factor in the blend than in either of the two pure materials. The fitting parameters shown in Table 1 suggest *RR*-P3HT has a narrower DOS (1.2 K_BT compared with 4 K_BT) with slightly higher localization length (2.8Å>2Å) located at lower energies. The ratio in the DOS width (3.3) is similar to the scenario shown in the second column of Fig 4 (2.4), and as modeled for the higher mobility ratios there is an increase in the power factor.

Next, we examine the other two blend systems that are not expected to give rise to higher power factors. For the PDPP-4T:*RRa*-P3HT blend system, the charge-carrier mobility of *RRa*-P3HT is 3 to 4 orders of magnitude smaller than that in PDPP-4T, and thus the contribution of PDPP-4T is likely to dominate over *RRa*-P3HT in determining the power factor. Indeed, the 3+ order of magnitude difference in the electrical conductivity and the higher Seebeck coefficient for PDPP-4T leads to PDPP-4T dominating transport and the power factor in the blends. The fitting parameters for the PDPP-4T and *RRa*-P3HT blends (Table 1) suggest that PDPP-4T has a broader DOS with higher localization length at higher energies (details of fitting parameter determination can be found in the SI).

The final blend system we examine is PDPP-4T:PDPP-T-TT-T, where there is almost no charge-carrier mobility difference. Surprisingly, the electrical conductivity of PDPP-T-TT-T is much smaller than that of PDPP-4T (0.9 Sm^{-1} compared to 31.8 Sm^{-1}). Increasing the ratio of PDPP-4T in the blend leads to a constant decrease in *S* from 404 μVK^{-1} to 204 μVK^{-1}, which opposes the changes in electrical conductivity. The large Seebeck coefficient and low electrical conductivity in pure PDPP-T-TT-T suggests a low charge-carrier concentration and high total number of states, which agrees with the fitting parameters ($N_{t,PDPP\text{-}T\text{-}TT\text{-}T}=10^{21}cm^{-3}$ and $N_{C,PDPP\text{-}T\text{-}TT\text{-}T}=1.5\times10^{19}cm^{-3}$ or $\frac{N_{C,PDPP-T-TT-T}}{N_{t,PDPP-T-TT-T}} = 1.5\%$). Furthermore, the fitting parameters for these two polymers suggest we have blended two polymers with almost similar disorder and similar localization length with 0.08 eV energetic offset. This scenario can be best represented by the calculated data in SI Figure S5 when the mobility ratio is small, and as predicted by the model there is not any improvement in the power factor.

Photothermal deflection spectroscopy (PDS) measurements,[76,77] as shown in SI Figure S12, were carried

This journal is © The Royal Society of Chemistry 20xx
Please do not adjust margins

out in an effort to obtain experimental evidence into the DOS widths for the different polymers.[64] From these PDS spectra the Urbach energy was extracted, where the Urbach energy provides a quantitative measurement of the extent of disorder. Unfortunately, the polaron absorbance in the polymers extends beyond the limits of the PDS system and therefore the un-doped polymers were investigated. In the un-doped polymers, the Urbach energies of *RR*-P3HT, PDPP-4T, and PDPP-T-TT-T are similar at 42 to 45 meV, whereas *RRa*-P3HT is significantly higher at 170 meV. Considering that the Urbach energy should reflect the DOS width, these values are in disagreement with the values extracted through fitting the experimental data with the theoretical model. We suspect that this discrepancy arises from the PDS measurements being performed on the un-doped polymers. Adding chemical dopants has previously been shown both experimentally and theoretically to significantly alter the relative disorder and DOS widths in the polymers.[52–54,63] Experimentally probing disorder in these doped systems is a direction that we will pursue in future work.

There are three additional fitting parameters that differ between the polymers and have major contributions to the observed experimental trends. These include the total density of states, the density of charge carriers and attempt to jump frequency. The total number of states is equal to the total number of states that have some contribution to charge transport. The total number of states is highest for PDPP-T-TT-T (10×10^{20}cm^{-3}) and lowest for *RRa*-P3HT (2.96×10^{20}cm^{-3}) and their value can be affected by multiple parameters, including morphological factors that restrict transport or the presence of energetic traps. Despite keeping the concentration of the dopant constant (Table S1) in the films, the concentration of charge carriers is not the same for all polymers. *RR*-P3HT and *RRa*-P3HT have the highest charge carrier concentration (12×10^{19}cm^{-3}) versus PDPP-4T (6×10^{19}cm^{-3}) and PDPP-T-TT-T (1.5×10^{19}cm^{-3}). There are a few possible reasons for these differences, such as dopant aggregation[78,79] or lower energetic offsets between the EA of the dopant and IE of the polymer,[36] both of which can decrease the doping efficiency. The extracted charge-carrier concentration does correspond with the doping efficiency expected based purely on the IE of the polymers, with the carrier concentration decreasing as the polymer IE increases; however, it is difficult to experimentally verify the exact concentration of charge carriers. Attempt to jump frequency should be in order of 10^{11}-10^{13} s^{-1} (i.e., order of phonon vibration frequency), but the fitting parameters used to fit to our experimentally measured electrical conductivity are about two orders of magnitude higher. Predicting a correct prefactor for electrical conductivity has been a challenge for analytical models. [32,40,80,81]Here we have used a linear combination ν_0 of two pure polymers to fit to blend systems (Equation S19).AFM images of these polymer blends, as displayed in SI Figure S13, show large aggregates in both pure PDPP-T-TT-T and PDPP-4T films and in the blends at or above a PDPP-4T composition of 0.5. These aggregates are absent in the undoped polymer, and thereby we suspect that they are dopant rich, either consisting entirely of the dopant or consisting of highly doped polymers that are rendered insoluble upon heavy doping.[82] Dopant aggregation would also agree with lower carrier concentration in these DPP containing polymers as compared to both P3HT polymers. The morphology of the films can play a large role in determining the thermoelectric performance, particularly in polymer blends.[33] Importantly for comparison purposes, the blend systems in this work show similar aggregated morphologies at higher (>0.5) PDPP-4T compositions where the increased power factors are observed for the RR-P3HT:PDPP-4T blends. The analytical model presented provides a nice framework for understanding the thermoelectric properties of polymer blends, but moving forward it will be important to experimentally investigate the morphologies in detail and incorporate the influence of morphology into the theoretical model. For example, the current analytical model may be expanded to include a perturbation of the probability of hopping between the two polymers (C'_A and C'_B) based on the morphology.

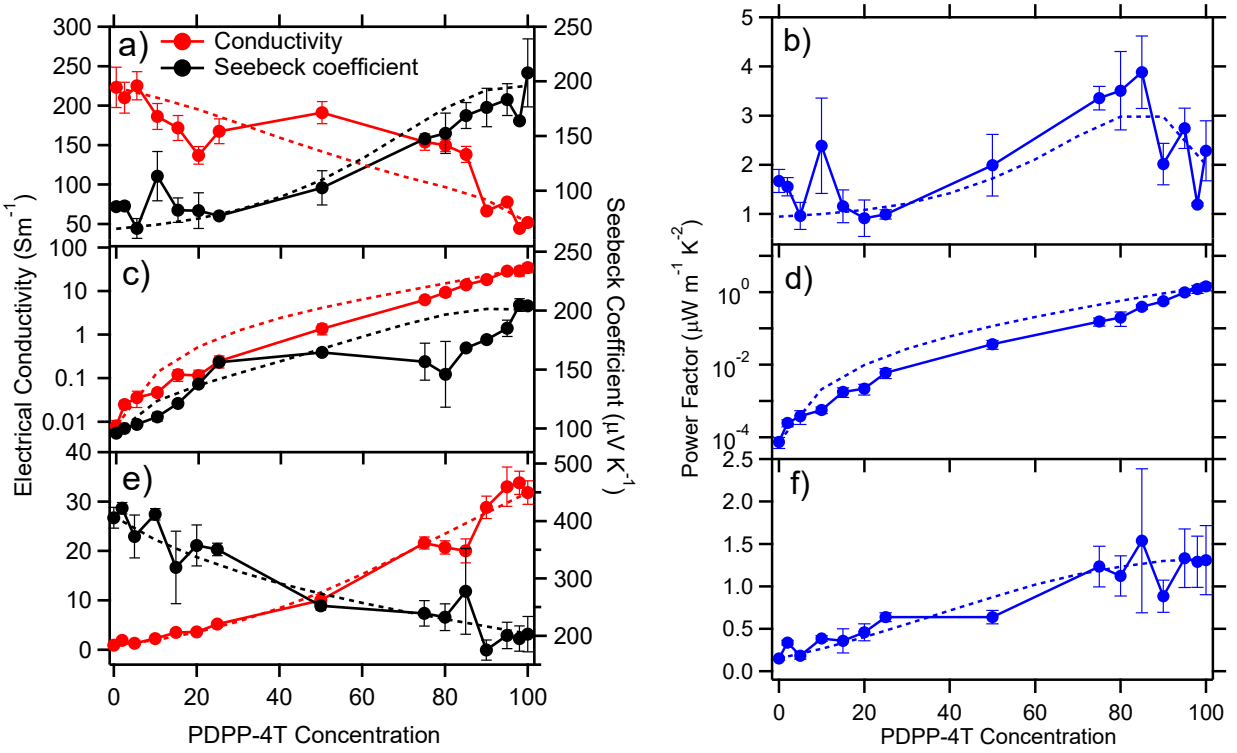

Figure 6. (a,c,e) Seebeck coefficient and electrical conductivity and (b,d,f) power factor as a function of PDPP-4T concentration in polymer blend. The blends are PDPP-4T:RR-P3HT (a,b) and PDPP-4T:RRa:P3HT (c,d) and PDPP-4T:PDPP-T-TT-T (e,f). Dashed lines are the fits to the model as calculated with equations 7 and 8. The fitting parameters can be found in Table 1.

Table 1. fitting parameters for each polymer in each individual blend system

PDPP-4T:RR-P3HT								
Polymer	Δ (K_BT)	α (Å)	a (nm)	N_t (10^{20} cm^{-3})	N_C (10^{19} cm^{-3})	a/α	E_0	ν_0 (10^{15} s^{-1})
PDPP-4T	4	2.8	1.4	3.64	6	5	0	3.52
RR-P3HT	1.2	2	1.5	2.96	12	12.5	-0.15	44.8
PDPP-4T:RRa-P3HT								
Polymer	Δ (K_BT)	α (Å)	a (nm)	N_t (10^{20} cm^{-3})	N_C (10^{19} cm^{-3})	a/α	E_0	ν_0 (10^{15} s^{-1})
PDPP-4T	4	2.5	1.4	3.64	6	5.6	0	5.43
RRa-P3HT	2	1.2	1.5	2.96	12	12.5	-0.15	2.41
PDPP-4T:PDPP-T-TT-T								
Polymer	Δ (K_BT)	α (Å)	a (nm)	N_t (10^{20} cm^{-3})	N_C (10^{19} cm^{-3})	a/α	E_0	ν_0 (10^{15} s^{-1})
PDPP-4T	3.5	2.5	1.35	4.06	6	5.4	0	4.06
PDPP-T-TT-T	4.5	1.8	1	10	1.5	10	0.08	2.83

This journal is © The Royal Society of Chemistry 20xx
Please do not adjust margins

ARTICLE

Conclusion

The results presented show that polymer blends are capable of reaching higher power factors than either of the individual polymers. For higher power factors to be realized in the blend, the polymer with its DOS centered at higher energies should have a broader DOS and higher charge-carrier mobility. Furthermore, the electrical conductivities of the two polymers should not be drastically different, as this leads to the polymer with the higher electrical conductivity dominating charge transport and minimizing the influence of the other polymer. From a simple experimental viewpoint of selecting candidate polymers, the polymers should have similar electrical conductivities (within an order of magnitude) and Seebeck coefficients (within a factor of two), and the polymer with the higher IE should have a higher mobility.

In terms of guiding the design of thermoelectric polymers, our results indicate that polymers with low energetic disorder (i.e., a narrow density of states distribution) and large localization lengths should be targeted for both polymer blends and pure polymers. In the case of blends, increases in performance should be obtainable regardless of the DOS width and localization length of the lower energy polymer, so long as the polymer with the higher energy DOS has a broader DOS and comparable or larger localization length. There are numerous factors that this work did not account for, such as the morphology of the polymer blends and the effects of blending polymers together on the width of the DOS of each individual polymer, that are likely to be important in determining the thermoelectric performance of polymer blends. Future work that accounts for morphology, doping induced disorder, and polymer interactions will be helpful in further guiding the design of polymer blend thermoelectrics.

Conflicts of interest

In accordance with our policy on Conflicts of interest please ensure that a conflicts of interest statement is included in your manuscript here. Please note that this statement is required for all submitted manuscripts. If no conflicts exist, please state that "There are no conflicts to declare".

ASSOCIATED CONTENT

Supporting Information. Experimental procedures, further details on the theoretical models, calculated Fermi energy variations with polymer blend composition, thermoelectric performance parameters as a function of polymer blend composition and charge-carrier mobility ratio, UV-Vis absorbance spectra, PDS spectra, an expanded theoretical treatment of the polymer blends, and details on the fitting parameters for the polymer blends. This material is available free of charge via the Internet at http://pubs.acs.org.

AUTHOR INFORMATION

Corresponding Author

* Kenneth.Graham@uky.edu

Author Contributions

The manuscript was written through contributions of all authors. All authors have given approval to the final version of the manuscript.

Funding Sources

American Chemical Society Petroleum Research Fund (Grant # 57619-DNI10). NSF CAREER Award, #1653909,

Acknowledgements

A.A., Z. L., and K.R.G acknowledge the donors of The American Chemical Society Petroleum Research Fund for partial support of this research. J.M and X. Luo are grateful for the support from the National Science Foundation (NSF CAREER Award, #1653909). We thank Yadong Zhang and Seth R. Marder for supplying $Mo(tfd)_3$.

ABBREVIATIONS

S: Seebeck coefficient; σ: electrical conductivity; α: localization length; a: intrinsic length; DOS: density of states.

Notes and references

1 2017_United-States_Energy.pdf, https://flowcharts.llnl.gov/commodities/energy.

2 J. He and T. M. Tritt, *Science.*, 2017, **357**, eaak9997.

3 S. K. Yee, S. Leblanc, K. E. Goodson and C. Dames, *Energy Environ. Sci.*, 2013, **6**, 2561–2571.

4 G. J. Snyder and E. S. Toberer, *Nat. Mater.*, 2008, **7**, 105–114.

5 S. Lin, W. Li, Z. Chen, J. Shen, B. Ge and Y. Pei, *Nat. Commun.*, 2016, **7**, 10287.

6 B. Russ, A. Glaudell, J. J. Urban, M. L. Chabinyc and R. A. Segalman, *Nat. Rev. Mater.*, 2016, **1**, 16050.
7 Y. Du, J. Xu, B. Paul and P. Eklund, *Appl. Mater. Today*, 2018, **12**, 366–388.
8 C. Wang, K. Sun, J. Fu, R. Chen, M. Li, Z. Zang, X. Liu, B. Li, H. Gong and J. Ouyang, *Adv. Sustain. Syst.*, 2018, **2**, 1800085.
9 S. J. Kim, J. H. We and B. J. Cho, *Energy Environ. Sci.*, 2014, **7**, 1959–1965.
10 O. Bubnova and X. Crispin, *Energy Environ. Sci.*, 2012, **5**, 9345–9362.
11 M. Bharti, A. Singh, S. Samanta and D. K. K. Aswal, *Prog. Mater. Sci.*, 2018, **93**, 270–310.
12 D. Kiefer, L. Yu, E. Fransson, A. Gómez, D. Primetzhofer, A. Amassian, M. Campoy-Quiles and C. Müller, *Adv. Sci.*, 2017, **4**, 1600203.
13 S. W. Angrist, *Direct energy conversion*, Allyn and Bacon, Boston, MA, 1977.
14 J. C. Duda, P. E. Hopkins, Y. Shen and M. C. Gupta, *Appl. Phys. Lett.*, 2013, **102**, 251912.
15 J. W. Brill, M. Shahi, M. M. Payne, J. Edberg, Y. Yao, X. Crispin and J. E. Anthony, *J. Appl. Phys.*, 2015, **118**, 235501.
16 R. Kroon, D. A. Mengistie, D. Kiefer, J. Hynynen, J. D. Ryan, L. Yu and C. Müller, *Chem. Soc. Rev.*, 2016, **45**, 6147–6164.
17 B. T. McGrail, A. Sehirlioglu and E. Pentzer, *Angew. Chemie - Int. Ed.*, 2015, **54**, 1710–1723.
18 Q. Zhang, Y. Sun, W. Xu and D. Zhu, *Adv. Mater.*, 2014, **26**, 6829–6851.
19 G.-H. Kim, L. Shao, K. Zhang and K. P. Pipe, *Nat. Mater.*, 2013, **12**, 719–23.
20 S. Van Reenen and M. Kemerink, *Org. Electron.*, 2014, **15**, 2250–2255.
21 M. Culebras, C. Gómez and A. Cantarero, *Materials (Basel).*, 2014, **7**, 6701–6732.
22 O. Bubnova, Z. U. Khan, A. Malti, S. Braun, M. Fahlman, M. Berggren and X. Crispin, *Nat. Mater.*, 2011, **10**, 429–433.
23 J. Liu, L. Qiu, G. Portale, M. Koopmans, G. ten Brink, J. C. Hummelen and L. J. A. Koster, *Adv. Mater.*, 2017, **29**, 1701641.
24 Q. Zhang, Y. Sun, W. Xu and D. Zhu, *Energy Environ. Sci.*, 2012, **5**, 9639.
25 J. Hynynen, E. Järsvall, R. Kroon, Y. Zhang, S. Barlow, S. R. Marder, M. Kemerink, A. Lund and C. Müller, *ACS Macro Lett.*, 2019, **8**, 70–76.
26 Z. Liang, Y. Zhang, M. Souri, X. Luo, A. M. Boehm, R. Li, Y. Zhang, T. Wang, D.-Y. Kim, J. Mei, S. R. Marder and K. R. Graham, *J. Mater. Chem. A*, 2018, **6**, 16495–16505.
27 A. M. Glaudell, J. E. Cochran, S. N. Patel and M. L. Chabinyc, *Adv. Energy Mater.*, 2015, **5**, 1401072.
28 I. E. Jacobs, E. W. Aasen, J. L. Oliveira, T. N. Fonseca, J. D. Roehling, J. Li, G. Zhang, M. P. Augustine, M. Mascal and A. J. Moulé, *J. Mater. Chem. C*, 2016, **4**, 3454–3466.
29 K. Shi, F. Zhang, C.-A. Di, T.-W. Yan, Y. Zou, X. Zhou, D. Zhu, J.-Y. Wang and J. Pei, *J. Am. Chem. Soc.*, 2015, **137**, 6979–6982.
30 J. Liu, G. Ye, B. van der Zee, J. Dong, X. Qiu, Y. Liu, G. Portale, R. C. Chiechi and L. J. A. Koster, *Adv. Mater.*, 2018, **30**, 1804290.
31 J. Sun, M.-L. Yeh, B. J. Jung, B. Zhang, J. Feser, A. Majumdar and H. E. Katz, *Macromolecules*, 2010, **43**, 2897–2903.
32 G. Zuo, H. Abdalla and M. Kemerink, *Adv. Electron. Mater.*, 2019, 1800821.
33 G. Zuo, X. Liu, M. Fahlman and M. Kemerink, *ACS Appl. Mater. Interfaces*, 2018, **10**, 9638–9644.
34 D. Yoo, J. Kim and J. H. Kim, *Nano Res.*, 2014, **7**, 717–730.
35 D. Yoo, J. Kim, S. H. Lee, W. Cho, H. H. Choi, F. S. Kim and J. H. Kim, *J. Mater. Chem. A*, 2015, **3**, 6526–6533.
36 G. Zuo, X. Liu, M. Fahlman and M. Kemerink, *Adv. Funct. Mater.*, 2018, **28**, 1703280.
37 I. V. Arkhipov, P. Heremans, E. V. Emelianova, G. J. Adriaenssens and H. Bässler, *J. Phys. Condens. Matter*, 2002, **14**, 9899–9911.
38 A. Miller and E. Abrahams, *Phys. Rev.*, 1960, **120**, 745–755.
39 N. F. Mott, *Philos. Mag.*, 1968, **17**, 1259–1268.
40 G. Zuo, H. Abdalla and M. Kemerink, *Phys. Rev. B*, 2016, **93**, 235203.
41 I. I. Fishchuk, V. I. Arkhipov, A. Kadashchuk, P. Heremans and H. Bässler, *Phys. Rev. B*, 2007, **76**, 1–12.
42 H. . Bässler, *Phys. Status Solidi*, 1993, **175**, 15–56.
43 I. I. Fishchuk, A. Kadashchuk, L. Sudha Devi, P. Heremans, H. Bässler and A. Köhler, *Phys. Rev. B.*, 2008, **78**, 1–8.
44 Y. Roichman and N. Tessler, *Appl. Phys. Lett.*, 2002, **80**, 1948–1950.
45 N. Lu, L. Li and M. Liu, *Phys. Rev. B*, 2015, **91**, 1–5.
46 D. Mendels and N. Tessler, *J. Phys. Chem. Lett.*, 2014, **5**, 3247–3253.
47 N. Tessler, Y. Preezant, N. Rappaport and Y. Roichman, *Adv. Mater.*, 2009, **21**, 2741–2761.
48 Y. Xuan, X. Liu, S. Desbief, P. Leclère, M. Fahlman, R. Lazzaroni, M. Berggren, J. Cornil, D. Emin and X. Crispin, *Phys. Rev. B*, 2010, **82**, 1–9.
49 J. L. Brédas, R. R. Chance and R. Silbey, *Phys. Rev. B*, 1982, **26**, 5843–5854.
50 E. F. Valeev, V. Coropceanu, D. A. da Silva Filho, S. Salman and J.-L. Brédas, *J. Am. Chem. Soc.*, 2006, **128**, 9882–9886.
51 N. Lu, L. Li and M. Liu, *Phys. Chem. Chem. Phys.*, 2016, **18**, 19503–19525.
52 E. M. Thomas, B. C. Popere, H. Fang, M. L. Chabinyc and R. A. Segalman, *Chem. Mater.*, 2018, **30**, 2965–2972.
53 V. I. Arkhipov, P. Heremans, E. V. Emelianova and H. Bässler, *Phys. Rev. B*, 2005, **71**, 1–7.
54 H. Abdalla, G. Zuo and M. Kemerink, *Phys. Rev. B*, 2017, **96**, 241202.
55 A. J. Heeger, *Rev. Mod. Phys.*, 2001, **73**, 681.
56 V. Coropceanu, J. Cornil, D. A. da Silva Filho, Y. Olivier, R. Silbey and J.-L. Brédas, *Chem. Rev.*, 2007, **107**, 926–952.
57 S. Dongmin Kang and G. Jeffrey Snyder, *Nat. Mater.*, 2017, **16**, 252–257.
58 A. V Nenashev, J. O. Oelerich and S. D. Baranovskii, *J. Phys. Condens. Matter*, 2015, **27**, 093201.
59 I. I. Fishchuk, A. K. Kadashchuk, J. Genoe, M. Ullah, H. Sitter, T. B. Singh, N. S. Sariciftci and H. Bässler, *Phys. Rev. B* , 2010, **81**, 1–12.
60 I. G. Austin and N. F. Mott, *Adv. Phys.*, 2001, **50**, 757–812.

This journal is © The Royal Society of Chemistry 20xx

Please do not adjust margins

61 T. Sato, H. Kinjo, J. Yamazaki and H. Ishii, *Appl. Phys. Express*, 2017, **10**, 011602.

62 V. I. Arkhipov, J. Reynaert, Y. D. Jin, P. Heremans, E. V. Emelianova, G. J. Adriaenssens and H. Bässler, *Synth. Met.*, 2003, **138**, 209–212.

63 V. I. Arkhipov, E. V. Emelianova, P. Heremans and H. Bässler, *Phys. Rev. B*, 2005, **72**, 235202.

64 D. Venkateshvaran, M. Nikolka, A. Sadhanala, V. Lemaur, M. Zelazny, M. Kepa, M. Hurhangee, A. J. Kronemeijer, V. Pecunia, I. Nasrallah, I. Romanov, K. Broch, I. McCulloch, D. Emin, Y. Olivier, J. Cornil, D. Beljonne and H. Sirringhaus, *Nature*, 2014, **515**, 384–388.

65 H. C. F. Martens, P. W. M. Blom and H. F. M. Schoo, *Phys. Rev. B*, 2000, **61**, 7489–7493.

66 V. I. Arkhipov, P. Heremans, E. V. Emelianova, G. J. Adriaenssens and H. Bässler, *Appl. Phys. Lett.*, 2003, **82**, 3245–3247.

67 K. R. Graham, G. O. N. Ndjawa, S. M. Conron, R. Munir, K. Vandewal, J. J. Chen, S. Sweetnam, M. E. Thompson, A. Salleo, M. D. McGehee and A. Amassian, *Adv. Energy Mater.*, 2016, **6**, 1601211.

68 M. L. Tietze, W. Tress, S. Pfützner, C. Schünemann, L. Burtone, M. Riede, K. Leo, K. Vandewal, S. Olthof, P. Schulz and A. Kahn, *Phys. Rev. B*, 2013, **88**, 085119.

69 J. Sun, M.-L. Yeh, B. J. Jung, B. Zhang, J. Feser, a. Majumdar and H. E. Katz, *Macromolecules*, 2010, **43**, 2897–2903.

70 P. Reiser, L. Müller, V. Sivanesan, R. Lovrincic, S. Barlow, S. R. Marder, A. Pucci, W. Jaegermann, E. Mankel and S. Beck, *J. Phys. Chem. C*, 2018, **122**, 14518–14527.

71 G. Wang, J. Swensen, D. Moses and A. J. Heeger, *J. Appl. Phys.*, 2003, **93**, 6137–6141.

72 P. H. Chu, G. Wang, B. Fu, D. Choi, J. O. Park, M. Srinivasarao and E. Reichmanis, *Adv. Electron. Mater.*, 2016, **2**, 1–12.

73 Y. Zhao, X. Zhao, M. Roders, G. Qu, Y. Diao, A. L. Ayzner and J. Mei, *Chem. Mater.*, 2015, **27**, 7164–7170.

74 B. C. Schroeder, T. Kurosawa, T. Fu, Y.-C. Chiu, J. Mun, G.-J. N. Wang, X. Gu, L. Shaw, J. W. E. Kneller, T. Kreouzis, M. F. Toney and Z. Bao, *Adv. Funct. Mater.*, 2017, **27**, 1701973.

75 S. A. Paniagua, J. Baltazar, H. Sojoudi, S. K. Mohapatra, S. Zhang, C. L. Henderson, S. Graham, S. Barlow and S. R. Marder, *Mater. Horizons*, 2014, **1**, 111–115.

76 B. Couch, A. Meyer, B. Heller and S. L. Johnson, *Methods Appl. Fluoresc.*, 2018, **7**, 015004.

77 W. B. Jackson, N. M. Amer, A. C. Boccara and D. Fournier, *Appl. Opt.*, 1981, **20**, 1333.

78 M. M. Said, Y. Zhang, R. R. Dasari, D. H. Anjum, R. Munir, H. Hu, A. Amassian, S. Barlow and S. R. Marder, *Org. Photonics Photovolt.*, 2016, **4**, 1–16.

79 J. Euvrard, A. Revaux, P. A. Bayle, M. Bardet, D. Vuillaume and A. Kahn, *Org. Electron.*, 2018, **53**, 135–140.

80 G. Kim and K. P. Pipe, *Phys. Rev. B*, 2012, **86**, 1–5.

81 I. I. Fishchuk, H. Bässler, A. Köhler, J. Genoe and A. Kadashchuk, *Phys. Rev. Applied*, 2018, **10**, 054063.

82 I. E. Jacobs, E. W. Aasen, D. Nowak, J. Li, W. Morrison, J. D. Roehling, M. P. Augustine and A. J. Moulé, *Adv. Mater.*, 2017, **29**, 1603221.

This journal is © The Royal Society of Chemistry 20xx

ARTICLE

TOC

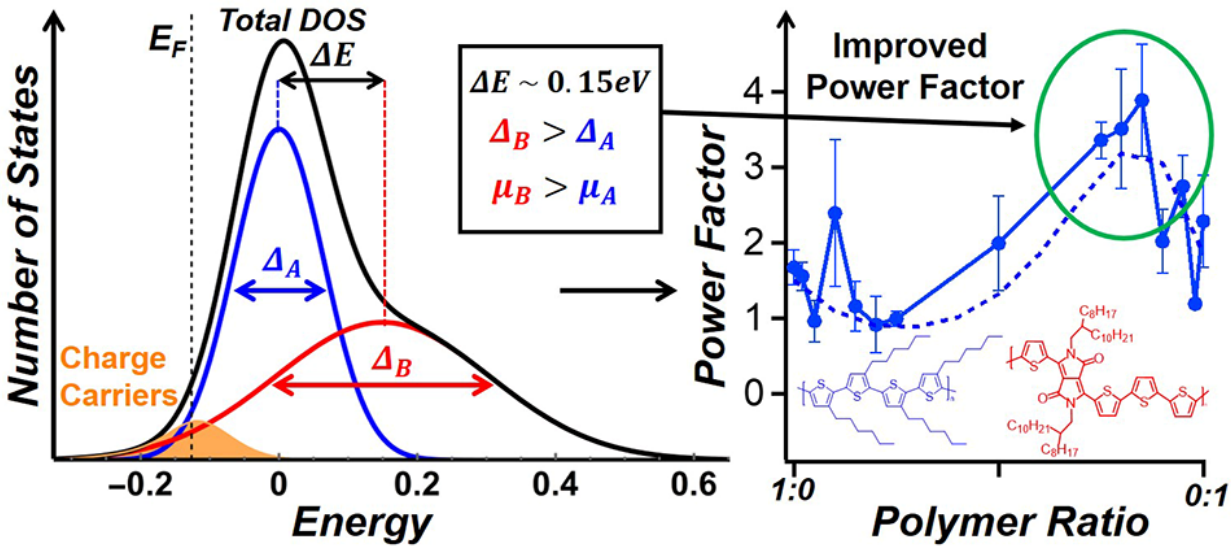
Number of States
E_F
Total DOS
ΔE
$\Delta E \sim 0.15eV$
$\Delta_B > \Delta_A$
$\mu_B > \mu_A$
Δ_A
Δ_B
Charge Carriers
−0.2
0
0.2
0.4
0.6
Energy
Improved Power Factor
Power Factor
4
3
2
1
0
1:0
0:1
Polymer Ratio